Remote Sensing of Vertical Velocity Variance and Surface Heat Flux in a Convective Boundary Layer

WAYNE M. ANGEVINE

CIRES, NOAA Aeronomy Laboratory/University of Colorado, Boulder, Colorado

RICHARD J. DOVIAK

National Severe Storms Laboratory, Norman, Oklahoma

ZBIGNIEW SORBJAN

School of Meteorology, University of Oklahoma, Norman, Oklahoma

(Manuscript received 26 July 1993, in final form 15 November 1993)

ABSTRACT

The vertical velocity variance in the convective atmospheric boundary layer is estimated from measurements made with a 915-MHz boundary layer wind-profiling radar. The vertical velocity variance estimates are used to infer the surface virtual heat flux through a relationship with the convective velocity scale w_*. The flux estimates are compared with in situ surface flux measurements and estimates extrapolated to the surface from direct eddy correlation measurements made with a profiler and radio acoustic sounding system. The measurements were made during the Rural Oxidants in the Southern Environment II Experiment in June 1992. The experiment area is primarily pine forest, and the dominant weather conditions were hot with light winds. The profiler variance measurements are compatible with theory and earlier observations. Both remote radar methods of estimating surface virtual heat flux agree with in situ measurements to within the sampling uncertainty.

1. Introduction

Measurements of atmospheric boundary layer turbulence are needed for many applications, such as chemical and air pollution studies and mesoscale and synoptic-scale modeling, but these measurements are generally difficult and expensive. The boundary layer profiler is a new instrument that has considerable promise for making such measurements continuously at reduced expense for both intensive campaigns and long-term studies. Angevine et al. (1993a; 1993b) report direct eddy correlation measurements of virtual heat flux in the convective atmospheric boundary layer with a 915-MHz boundary layer profiler–radio acoustic sounding system (profiler–RASS). This paper reports measurements of vertical velocity variance and surface virtual heat flux. The surface flux is estimated by two remote sensing methods: first by using its relationship to the vertical velocity variance σ_w^2 through the convective velocity scale w_*, and second by extrapolating the eddy correlation measurements to the surface. Flux measurements taken in the traditional way by a sonic anemometer are used for comparison. The data were taken during the Rural Oxidants in the Southern Environment II (ROSE II) Experiment near Jachin, Alabama, in June 1992.

The turbulent virtual heat flux is defined as

$$Q_v = \rho C_p \overline{w'\theta_v'}, \tag{1}$$

where w' is the perturbation of vertical velocity, θ_v' is the perturbation of virtual potential temperature, ρ is the air density, and C_p is the specific heat, which is assumed constant. The virtual heat flux is the primary driver of boundary layer mixing under unstable conditions with light winds (Stull 1988) and is therefore of interest in any boundary layer observation or modeling program.

The upward turbulent transport of heat and moisture from the earth's surface can be estimated in several ways. Some methods (based on Monin–Obukhov similarity theory) require measurements of wind, temperature, and humidity at a few altitudes within the surface layer, and others (based on resistance laws) require synoptic information. Both types of methods provide indirect measures of the surface heat flux (Sorbjan 1989). An in situ direct measure of virtual heat flux can be obtained by correlating collocated measurements of temperature, humidity, and vertical velocity (Lenschow 1986).

Corresponding author address: Wayne M. Angevine, NOAA Aeronomy Laboratory, R/E/AL3, 325 Broadway, Boulder, CO 80303.

In situ ground-based measurements depend on local terrain features and may not be representative of area averages pertinent to many meteorological problems. Remote sensors enable estimation of a spatial distribution of atmospheric parameters over large areas. Consequently, they could provide more stable and reliable estimates of mean fluxes than single-point sensors. It should be noted that the fixed (nonscanning) beam configuration of the profiler limits the number of independent measurements to the number of convective elements that pass through or evolve in the beam. Nevertheless, the vertically or nearly vertically pointed beam samples a volume of the order of 10^5 m^3 depending on the range and on the mean wind speed (see section 2a). Sampling over a larger volume than with in situ instruments should produce measurements that are representative of a larger area. On the other hand, the characteristic scale of the convective elements is larger in the mixed layer than in the surface layer, requiring a longer sampling time for a representative time average (see section 4).

The ROSE II site was within a managed pine forest. Sections of the forest had been cut and replanted at various times, leaving a patchwork of various sizes of trees. The profiler–RASS was located in an area that had been cleared about four years before and had pine trees about 2 m high and other lower brush. Weather conditions were ideal during the period when the aircraft and surface instruments were operating (18–25 June 1992), with clear to partly cloudy skies and no rainfall during midday.

The 915-MHz profiler was designed at the National Oceanic and Atmospheric Administration (NOAA) Aeronomy Laboratory (Ecklund et al. 1988) and is now commonly used for wind profiling in the boundary layer. A RASS is made up of a Doppler radar—in this case, the profiler—and one or more acoustic sources (Matuura et al. 1986; May et al. 1988; May et al. 1990). The acoustic sources are located near the radar antenna, and the radar measures the speed at which the acoustic wave propagates. The speed of sound is proportional to the square root of virtual temperature. If the air is moving along the beam, the apparent sound speed will be changed, so it is necessary to measure and correct for the radial wind velocity. With the recent addition of the capability to measure the radial wind velocity and acoustic velocity simultaneously when used as a RASS (Angevine et al. 1994a), the components needed for eddy correlation flux measurements are now available.

The profiler used in the ROSE II experiments operated at 915 MHz with a 1.8-m-square four-panel microstrip patch array antenna and 500 W of peak power. The one-way half-power beamwidth was 9°. The RASS acoustic power was 30 W. The antenna was mechanically steered into five beam positions, one vertical and four oblique positions 12° off zenith in two perpendicular planes. The oblique beam positions allowed the system to operate as a wind profiler as well as to measure the temperature profile and buoyancy flux. Both acoustic and radial wind velocities were measured in all beam positions. An aluminum honeycomb clutter fence was used to reduce ground clutter from nearby trees.

2. Technique

a. Profiler operation and sampling

The profiler sampled resolution volumes along each beam position for 30 s and then spent 10 s performing calculations and allowing the antenna to move to a new pointing direction and stabilize. Therefore, a profile of radial velocity was available every 40 s. The range resolution was 105 m, and the lowest resolution volume was centered at 150 m. The profiler averages air motions and temperature in a resolution volume defined in the along-beam direction by the range resolution; in the direction along the wind by the beamwidth plus the product of wind velocity and sampling time; and in the crosswind direction by the beamwidth. For example, if the wind speed is 2 m s^{-1}, the resolution cell dimensions at 150-m range are 105 m vertical, 76 m [16 m + (30 s) (2 m s^{-1})] along the wind, and 16 m crosswind.

b. Profiler data quality control

The raw profiler data contain both correct and incorrect estimates of the wind and acoustic velocities. Bad velocity estimates may be due to ground clutter, birds, insects, aircraft, poor return signal power, rain, or radio-frequency interference. Before the data can be used to calculate flux, the velocity time series must be cleaned to remove bad data points. Commonly used profiler data cleaning algorithms rely on continuity in height and/or time to distinguish bad data from good. That is, good velocity estimates are taken to be those that are reasonably similar to estimates above, below, before, and after the particular height and time in question. In the turbulent convective boundary layer, this assumption is not generally valid. The size of the radar resolution cell is within the range of scales of active turbulence, and so individual measurements are expected to differ substantially, even in adjacent heights and times.

The approach used on the data presented here is to accept data that fall within statistical limits. The limits are applied to each of the parameters available from the profiler—that is, to the signal-to-noise ratio (SNR), the velocity, and the width of the Doppler spectra. The data are divided into 2-h segments that contain about 180 individual measurements for each height. The good measurements are those that fall within all of the following limits based on the mean, median, and standard deviation σ of the 2-h time series:

velocity:	median $\pm 3\sigma$
spectral width:	mean $\pm 2\sigma$
SNR:	mean $\pm 2\sigma$

These limits were chosen from examination of the distributions of the respective parameters, from examination of large numbers of individual spectra, and from physical arguments. For example, an unusually high clear-air SNR is probably due to an object such as a bird or aircraft.

c. *Vertical velocity variance estimation*

A complete measurement of the vertical velocity variance requires a combination of large- and small-scale measurements. The large-scale variance is computed from the time series of cleaned velocities. The small-scale variance is computed from the cleaned spectral width measurements.

Since the profiler operated in a five-beam cycle, a measurement on the vertical beam was available only for 30 s every 200 s. A vertical velocity estimate can be constructed from the radial velocities measured by coplanar pairs of oblique beams (northeast–southwest and northwest–southeast). The radial velocity measured by such an oblique beam is

$$v_r = v_h \sin\phi + w \cos\phi, \qquad (2)$$

where v_h is the horizontal velocity, w is the vertical velocity, and ϕ is the zenith angle. Combining vertical velocity estimates from coplanar beam pairs with the direct measurements from the vertical beam gives an average sampling period of 66 s. The small-scale and large-scale vertical velocity variance estimates will contain contributions from the horizontal velocity variance, but the oblique beams' zenith angle was only 12°. Therefore, the radial velocity contains 98% of the vertical velocity and only 21% of the horizontal velocity. At ROSE II in midday, the horizontal winds were generally light and the convective turbulence strong, and the horizontal and vertical variances as measured by aircraft were approximately the same. Including the oblique beam measurements significantly improved the correlation of the small-scale variance with w_*, probably because the sampling density and number of samples were increased.

1) Small-scale variance

Figure 1 shows the median spectral width squared for 2-h periods centered at 1100, 1200, and 1300 CST for 19–25 June. The height is normalized to the boundary layer height z_i estimated from the profiler (section 2e). The squared spectral width has an apparent floor of roughly 1.25 $m^2\ s^{-2}$. This floor is taken to be the system bias, which includes biases due to signal processing (such as window effects), meteorological mechanisms (e.g., mean wind) (Doviak and Zrnić 1993, section 5.2.2), artifacts (Doviak and Zrnić 1993, section 7.2), contributions from horizontal wind variance (because oblique beam data are used), and other unexplained mechanisms. In other words, we assume that the small-scale vertical velocity variance becomes negligibly small at the top of the mixed layer, and the minimum variance at that height is the contribution to spectral width caused by effects other than small-scale vertical velocity variance—that is, the system bias. When this bias is removed, the resulting spectral width is taken to be the small-scale radial velocity variance—that is, the variance on scales smaller than the resolution volume.

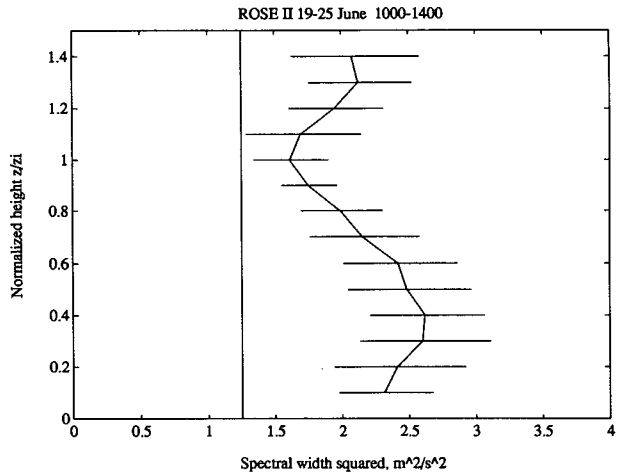

FIG. 1. Spectral width squared versus normalized height z/z_i. Medians for 2-h periods centered at 1100, 1200, and 1300 CST for each of 7 days, averaged over each 0.1 z/z_i interval, are shown. Horizontal bars are plus/minus one standard deviation. Straight line is the empirically selected system bias.

We have estimated the contributions to spectral width by mean flow that replenishes the scatterers within the resolution volume, by angular shear caused by the wind blowing across the finite-width beam, by the window effect, and by horizontal wind variance (estimated from aircraft measurements to be about equal to the vertical velocity variance). All of these effects combined to account for less than half of the system bias. We attribute the other half to artifacts and other unexplained effects.

2) Large-scale variance

The large-scale variances reported here also include vertical velocities derived from oblique beam pairs as well as the vertical beam. A linear trend was removed from each 2-h time series before computing the variance. Figure 2 shows the large-scale variance normalized to the convective velocity scale w_* versus normalized height, and Fig. 3 shows the total variance on all scales. In both figures, the variance profile has the

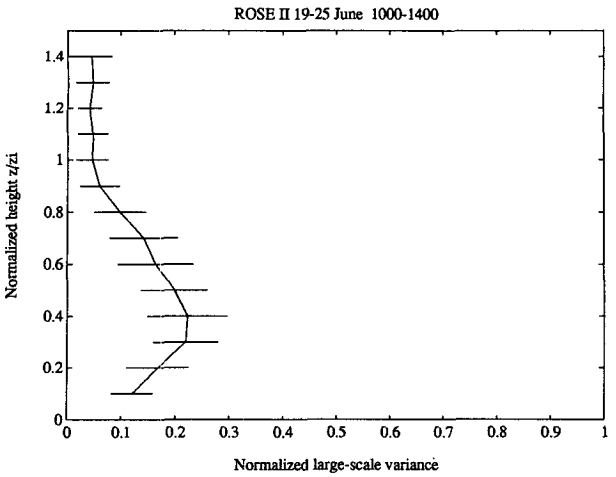

FIG. 2. Large-scale vertical velocity variance from the profiler normalized to w_*^2 versus normalized height. Two-hour averages centered at 1100, 1200, and 1300 CST for each of 7 days, averaged over each 0.1 z/z_i interval, are shown. Horizontal bars are plus/minus one standard deviation.

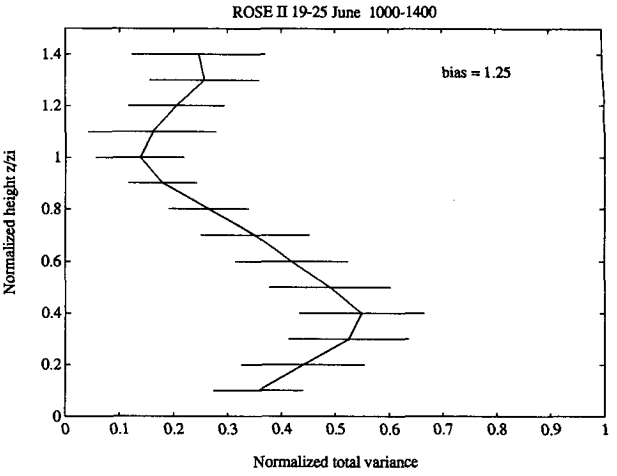

FIG. 3. Total vertical velocity variance from the profiler (large and small scale) normalized to w_*^2 vs normalized height. Two-hour averages centered at 1100, 1200, and 1300 CST for each of 7 days, averaged over each 0.1 z/z_i interval, are shown. Horizontal bars are plus/minus one standard deviation.

expected shape, peaking at roughly the middle of the mixed layer and dropping off near and above the boundary layer top. The range of the total variance (Fig. 3) is also consistent with the observations summarized by Stull (1988, Fig. 4.2).

The w_* values measured during the experiment period ranged from 1.6 to 2.4 m s^{-1}. The sonic anemometer was on a tower just above the forest canopy, about 500 m from the profiler site.

d. *Convective velocity scale* w_*

The convective velocity scale w_* is defined as

$$w_* = \left[\frac{gz_i}{\overline{\theta_v}}(\overline{w'\theta_v'})_s\right]^{1/3}, \qquad (3)$$

where g is the acceleration due to gravity, z_i is the boundary layer height, θ_v is the virtual potential temperature, and the subscript s denotes a quantity at the surface and since w_* contains the surface virtual heat flux, the boundary layer height can be derived from the profiler data (see below), and the other parameters are generally available; a remote measurement of w_* provides a means of estimating the surface virtual heat flux.

Vertical velocity variance in the mixed layer can be used to estimate w_*. Various published data (Sorbjan 1990, 1991; Kaimal et al. 1976; Moeng 1984; Caughey and Palmer 1979; Willis and Deardorff 1974; Yamada and Mellor 1975) can be used to estimate the relationship. Figure 4 shows the total vertical velocity variance from the ROSE II data averaged over 0.2–0.5 z_i plotted versus w_*^2. Averaging over this height range reduces the scatter in the result. The correlation coefficient is 0.74, which is significant at a confidence level of better than 99.9%. The average ratio of σ_w^2 to w_*^2 gives the relationship

$$\sigma_w^2 = 0.52w_*^2; \quad 0.2 < \frac{z}{z_i} < 0.5 \qquad (4)$$

for use in the comparisons that follow. The constant 0.52, which is toward the large end of the range of values found in the literature, is due to the inclusion of large scales (up to 2 h) in the measurement (Sorbjan 1991).

e. *Boundary layer height*

The convective boundary layer (CBL) height at midday on the days discussed here was 1100–1600 m.

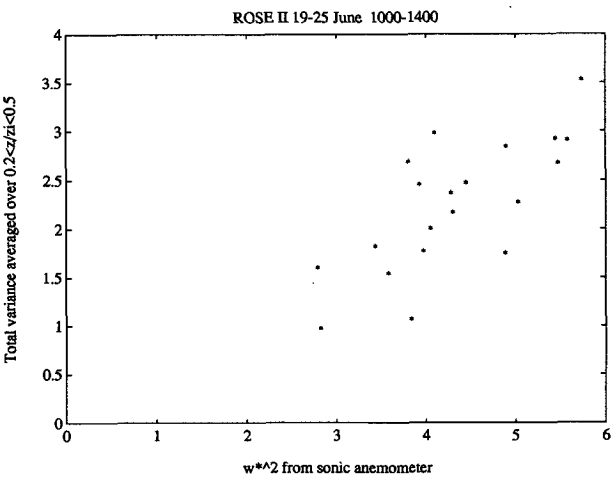

FIG. 4. Vertical velocity variance from the profiler averaged over 0.2–0.5 z/z_i for each 2-h period versus w_*^2.

The height is deduced from the SNR recorded by the profiler (Angevine et al. 1994b). White et al. (1991) cover the theory of this measurement in detail, so we will discuss it only briefly here. A clear-air radar such as the boundary layer profiler receives its return signal primarily from inhomogeneities of the radio refractive index. These inhomogeneities are characterized by the refractive-index structure parameter C_n^2. The profiler SNR at a given range is directly proportional to C_n^2 (Ottersten 1969; VanZandt et al. 1978). Wyngaard and LeMone (1980) show that C_n^2 peaks at the inversion atop a CBL. Therefore, a peak in the range-corrected SNR indicates the CBL top z_i.

f. Surface virtual heat flux from vertical velocity variance

Combining (1), (3), and (4), we solve for the surface virtual heat flux:

$$Q_{vs} = \frac{C_p \rho \theta_v}{g z_i} \left[\frac{\langle \sigma_w^2 \rangle}{0.52} \right]^{3/2}. \quad (5)$$

g. Surface virtual heat flux from eddy correlation

For the eddy correlation virtual heat flux measurement (Angevine et al. 1993a; Angevine et al. 1993b), the time series of temperature is computed using both the acoustic and clear-air velocities. A linear trend is removed from the time series of temperature and radial wind. The heat flux is then calculated by the method of Peters et al. (1985). In this method, the correlation of temperature and vertical velocity is computed at plus and minus one lag, and these results are averaged to give the correlation estimate. The Peters method is needed because any errors that remain in the clear-air velocity measurements after cleaning will show up as a reduction of the apparent correlation at zero lag, since the vertical velocity enters into the correlation both as itself and in the corrected temperature. The minimum fully resolvable scale in the along-wind direction is therefore twice the resolution cell size in that direction, or 152 m in the above example (2 m s^{-1} wind). To estimate the surface virtual heat flux, the eddy correlation measurements are extrapolated to the surface using a linear least-squares fit to each 2-h flux profile.

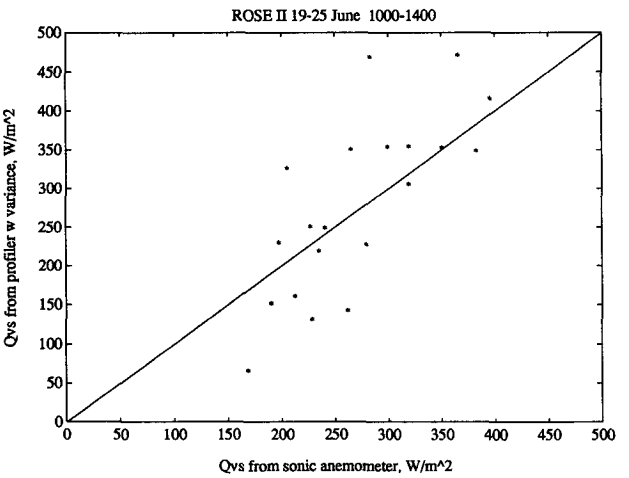

FIG. 5. Surface virtual heat flux estimated from profiler vertical velocity variance using Eq. (5) versus near-surface sonic anemometer measurement of Q_{vs}. Solid line is 1:1.

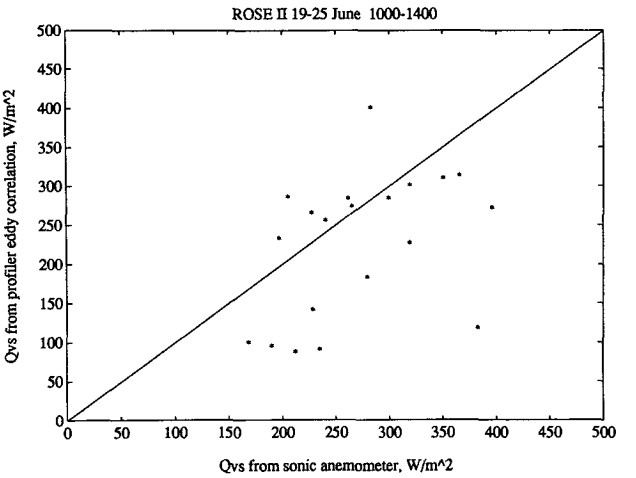

FIG. 6. As Fig. 5 but for surface virtual heat flux estimated by extrapolating profiler–RASS eddy correlation measurements to the surface.

3. Results

Figure 5 shows the surface virtual heat flux estimated from the mid-BL vertical velocity variance plotted versus the flux computed from the in situ sonic anemometer measurements of virtual temperature and vertical velocity. There is substantial scatter in the data, the ratio having a standard deviation of 0.32. The correlation coefficient is 0.75, significant at more than 99.9% confidence.

Figure 6 shows the surface virtual heat flux estimated from the direct eddy correlation measurements by the profiler plotted versus the flux from the sonic anemometer. The profiler estimates are about 15% low on average. The standard deviation of the ratio of the two flux measurements is 0.32. The correlation coefficient is 0.41, significant at 90% confidence. The exact agreement between the standard deviations of the two comparisons (Figs. 5 and 6) is coincidental.

4. Discussion

Time-average measurements such as those reported here are subject to considerable scatter because the energy-containing scales are large. An estimate of the uncertainty due to sampling for a finite time or distance is provided by the theoretical work of Wyngaard (1992)

and the experiments of Lenschow and Stankov (1986). The estimate is based on the time required for a time average to converge to within a certain limit of the ensemble average. The relative uncertainty e (the standard deviation divided by the mean) is

$$e^2 = \frac{2F\tau}{T}, \tag{6}$$

where τ is the integral scale in time of the flux, T is the averaging time, and

$$F = \frac{\overline{T_v'^2 w'^2} + (\overline{T_v' w'})^2}{(\overline{T_v' w'})^2} \tag{7}$$

for the eddy correlation heat flux estimate. For variances, $F = 2$. To determine the integral scale in time, we use the spatial integral-scale relationships measured by Lenschow and Stankov (1986):

$$\lambda_{wT} = 0.16 z^{1/3} z_i^{2/3} \tag{8}$$

for heat flux and

$$\lambda_{ww} = 0.16 z^{1/2} z_i^{1/2} \tag{9}$$

for vertical velocity variance; we apply Taylor's hypothesis to deduce $\tau = \lambda / U$, where U is the mean horizontal wind speed.

For the vertical velocity variance, we can use (9) with typical values of $z_i = 1300$ m, $z/z_i = 0.4$, and $U = 2$ m s^{-1} to arrive at an estimate of 70 s for the integral scale. Further, using (6), we can estimate the sampling uncertainty to be about 20% for the vertical velocity variance.

Given this estimate of the uncertainty in the measurement of the vertical velocity variance, we need to estimate the corresponding uncertainty in the computed virtual heat flux. Applying the standard formula for propagation of errors (Bevington 1969) to (5), we see that the relative uncertainty of the surface heat flux estimate is 3/2 times the relative uncertainty of the vertical velocity variance, or approximately 30%.

The estimation of sampling uncertainties for the eddy correlation flux estimate is somewhat more complex, since (7) must be used. Using the aircraft data from ROSE II, we estimate that typical integral scales τ_{wT} were 40–50 s and typical relative uncertainties were 30%–50% for a 2-h measurement (Angevine et al. 1993b). The aircraft flight legs considered were flown at 150–250 m AGL and all but one were flown before local noon, so the integral-scale estimates from the aircraft data will be less than those typical for the radar data, which are from higher heights and later times.

The relative uncertainty for the in situ measurements is 10%–20%, due to instrumental uncertainties (D. L. Matt 1993, personal communication).

All of the observed scatter in the surface flux estimate from the vertical velocity variance (Fig. 5) is accounted for by the uncertainty due to sampling and the instrumental uncertainty of the in situ flux measurement. This indicates that instrumental uncertainties in this method are certainly less than 30% and are probably considerably smaller. All of the observed scatter in the surface flux estimated from the profiler eddy correlation measurements can be attributed to the sampling uncertainty, indicating that instrumental uncertainties in that method are also less than 30%.

The profiler eddy correlation method measures 15% less flux than the surface instrument. Flux on scales less than about 100 m is not measured by this method. Comparison to aircraft measurements using the same dataset (Angevine et al. 1993b) shows that the neglect of these scales results in approximately the observed 15% underestimate.

The in situ surface measurement (sonic anemometer) may not be representative of the area as a whole. A study from the First ISLSCP (International Satellite Land Surface Climatology Project) Field Experiment (FIFE) (Smith et al. 1992) showed substantial differences between surface fluxes measured at different sites within a grassland area.

5. Conclusions

A method for estimating the vertical velocity variance in a convective boundary layer with a boundary-layer profiler was presented. The resulting variances are in good agreement with observations by other methods as well as theory and models.

Two methods of remotely estimating the surface virtual heat flux were presented, one using the vertical velocity variance and the other using eddy correlation. Both produce estimates that compare well with in situ sonic anemometer measurements. Either method may produce more representative measurements of the surface flux than an in situ measurement, especially over inhomogeneous terrain. The scatter in either method can be reduced by longer averaging under appropriate conditions.

Sampling uncertainties could be reduced by methods other than longer averaging. The techniques presented here may be applicable to other types of radars. Microwave radars or lidars could be mounted on aircraft to increase the number of independent samples per unit time. Scanning Doppler radars, such as the National Weather Service WSR-88D, could obtain large numbers of independent samples of velocity over large areas, especially if relationships were developed between radial velocity variance at large zenith angles and the surface virtual heat flux.

Acknowledgments. The surface data were graciously provided by Detleff Matt of NOAA Air Resources Laboratory, Atmospheric Turbulence and Diffusion Division, Oak Ridge, Tennessee. The members of the Tropical Dynamics and Climate Group of the NOAA Aeronomy Laboratory, under the direction of Ken Gage, assisted in the preparation of the profiler and in the analysis and discussion of the results. Jim Jordan

of NOAA WPL helped set up the profiler–RASS and provided the clutter fence. Partial funding for this study was provided by the Department of Energy Atmospheric Radiation Measurement program. ROSE II was conducted in collaboration with the Southern Oxidant Study.

REFERENCES

Angevine, W. M., S. K. Avery, W. L. Ecklund, and D. A. Carter, 1993a: Fluxes of heat and momentum measured with a boundary-layer wind profiler radar–radio acoustic sounding system. *J. Appl. Meteor.*, **32,** 73–80.

——, ——, and G. L. Kok, 1993b: Virtual heat flux measurements from a boundary-layer profiler–RASS compared to aircraft measurements. *J. Appl. Meteor.*, **32,** 1901–1907.

——, W. L. Ecklund, D. A. Carter, K. S. Gage, and K. P. Moran, 1994a: Improved radio acoustic sounding techniques. *J. Atmos. Oceanic Technol.*, **11,** 42–49.

——, A. B. White, and S. K. Avery, 1994b: Boundary layer depth and entrainment zone characterization with a boundary layer profiler. *Bound.-Layer Meteor.*, in press.

Bevington, P. R., 1969: *Data Reduction and Error Analysis for the Physical Sciences.* McGraw-Hill, 336 pp.

Caughey, S. J., and S. G. Palmer, 1979: Some aspects of turbulence structure through the depth of the convective boundary layer. *Quart. J. Roy. Meteor. Soc.*, **105,** 811–827.

Doviak, R. J., and D. S. Zrnić, 1993: *Doppler Radar and Weather Observations.* Academic Press, 562 pp.

Ecklund, W. L., D. A. Carter, and B. B. Balsley, 1988: A UHF wind profiler for the boundary layer: Brief description and initial results. *J. Atmos. Oceanic Technol.*, **5,** 432–441.

Kaimal, J. C., J. C. Wyngaard, D. A. Haugen, O. R. Cote, and Y. Izumi, 1976: Turbulence structure in the convective boundary layer. *J. Atmos. Sci.*, **33,** 2152–2169.

Lenschow, D. H., Ed., 1986: *Probing the Atmospheric Boundary Layer.* Amer. Meteor. Soc., 269 pp.

——, and B. B. Stankov, 1986: Length scales in the convective boundary layer. *J. Atmos. Sci.*, **43,** 1198–1209.

Matuura, N., Y. Masuda, H. Inuki, S. Kato, S. Fukao, T. Sato, and T. Tsuda, 1986: Radio acoustic measurement of temperature profile in the troposphere and stratosphere. *Nature,* **333,** 426–428.

May, P. T., R. G. Strauch, and K. P. Moran, 1988: The altitude coverage of temperature measurements using RASS with wind profiler radars. *Geophys. Res. Lett.*, **15,** 1381–1384.

——, ——, ——, and W. L. Ecklund, 1990: Temperature sounding by RASS with wind profiler radars: A preliminary study. *IEEE Trans. Geosci. Remote Sens.*, **28,** 19–28.

Moeng, C., 1984: A large-eddy-simulation model for the study of planetary boundary-layer turbulence. *J. Atmos. Sci.*, **41,** 2052–2062.

Ottersten, H., 1969: Atmospheric structure and radar backscattering in clear air. *Radio Sci.*, **4,** 1179–1193.

Peters, G., H. Hinzpeter, and G. Baumann, 1985: Measurements of heat flux in the atmospheric boundary layer by sodar and RASS: A first attempt. *Radio Sci.*, **6,** 1555–1564.

Smith, E. A., A. Y. Hsu, W. L. Crosson, R. T. Field, L. J. Fritschen, R. J. Gurney, E. T. Kanemasu, W. P. Kustas, D. Nie, W. J. Shuttleworth, J. B. Stewart, S. B. Verma, H. L. Weaver, and M. L. Wesely, 1992: Area-averaged surface fluxes and their time–space variability over the FIFE experimental domain. *J. Geophys. Res.*, **97,** 18 599–18 622.

Sorbjan, Z., 1989: *Structure of the Atmospheric Boundary Layer.* Prentice-Hall, 300 pp.

——, 1990: Similarity scales and universal profiles of statistical moments in the convective boundary layer. *J. Appl. Meteor.*, **29,** 762–775.

——, 1991: Evaluation of local similarity functions in the convective boundary layer. *J. Appl. Meteor.*, **30,** 1565–1583.

Stull, R. B., 1988: *An Introduction to Boundary-Layer Meteorology.* Kluwer, 666 pp.

VanZandt, T. E., V. L. Green, K. S. Gage, and W. L. Clark, 1978: Vertical profiles of refractivity turbulence structure constant: Comparison of observations by the Sunset Radar with a new theoretical model. *Radio Science,* **13,** 819–829.

White, A. B., C. W. Fairall, and D. W. Thompson, 1991: Radar observations of humidity variability in and above the marine atmospheric boundary layer. *J. Atmos. Oceanic Technol.*, **8,** 639–658.

Willis, G. E., and J. W. Deardorff, 1974: A laboratory model of the unstable planetary boundary layer. *J. Atmos. Sci.*, **31,** 1297–1307.

Wyngaard, J. C., 1992: Atmospheric turbulence. *Ann. Rev. Fluid Mech.*, **24,** 205–233.

——, and M. A. LeMone, 1980: Behavior of the refractive index structure parameter in the entraining convective boundary layer. *J. Atmos. Sci.*, **37,** 1573–1585.

Yamada, T., and G. Mellor, 1975: A simulation of the Wangara atmospheric boundary layer data. *J. Atmos. Sci.*, **32,** 2309–2329.